

STUDIES OF BEAM LOSS MONITORS AT THE CHINA SPALLATION NEUTRON SOURCE*

Tao Yang^{†,1}, Jilei Sun, Jianmin Tian, Lei Zeng, Taoguang Xu, Weiling Huang, Fang Li,
Zhihong Xu, Ruiyang Qiu, Ming Meng, Anxin Wang, Mengyu Liu¹, Xiaojun Nie
Institute of High Energy Physics, Chinese Academy of Sciences, Beijing, China
Spallation Neutron Source Science Center, Dongguan, China
¹also at University of Chinese Academy of Sciences, Beijing, China

Abstract

Beam loss detection is essential for the machine protection and the fine-tuning of the accelerator to reduce the induced radioactivity. The beam loss monitors (BLM) at the China Spallation Neutron Source (CSNS) are mainly divided into the following types: the coaxial cylindrical ionization chamber (IC) filled with Ar/N₂ gas mixture, Xe, BF₃ gas, and the scintillator with photomultipliers, among which the Ar/N₂ IC is the main type. In the low-energy section of the linac (beam energy <20 MeV), the BF₃ BLMs enclosed by a high-density polyethylene (HDPE) moderator are utilized to detect the beam losses. The Monte Carlo program FLUKA is employed to perform the relevant simulations. This paper presents the summary of the beam-loss detection for the CSNS BLM system.

INTRODUCTION

The CSNS had generated the neutron beam by the spallation reaction of 1.6-GeV protons striking on the tungsten target in August 2017. At present, its beam power is 100 kW with a repetition rate of 25 Hz. In phase II of CSNS, the beam power will be raised to 500 kW and the remaining neutron instruments will be built. A schematic layout of the CSNS phase I complex is shown in Fig. 1. The CSNS accelerator is mainly comprised of a 50-keV H⁺ ion source, a 3-MeV radio frequency quadrupole (RFQ) accelerator, an 80-MeV drift tube linac (DTL), and a 1.6 GeV proton rapid cycle synchrotron (RCS) [1]. The main design parameters of CSNS are listed in Table 1.

Table 1: The Basic Design Parameters of the CSNS

Design parameter	Value
Beam power (kW)	100
Linac energy (MeV)	80
Beam current in the linac (mA)	15
Extraction energy (GeV)	1.6
Proton per pulse	1.56×10^{13}
Repetition rate (Hz)	25
Linac RF frequency (MHz)	324
Target material	Tungsten

Beam loss may bring out high energy deposition to damage the accelerator components or produce undesired radioactivation, so it is one of the most important issues during

the running and commissioning of an accelerator facility [2-4]. Monitors based on the IC and plastic-scintillator with photomultipliers are the two types of BLMs used in the CSNS. There are 190 IC-type BLMs (preliminary and the subsequent newly added amount) along the entire beam line at the CSNS, mostly filled with Ar/N₂ mixture gas, several filled with Xe or BF₃ gas, and there are also 15 scintillator-based BLMs. IC is the main BLM type for the CSNS as well as other hadron machines due to its robustness to radiation damage, large dynamic range, little maintenance, and ease for calibration [5-8].

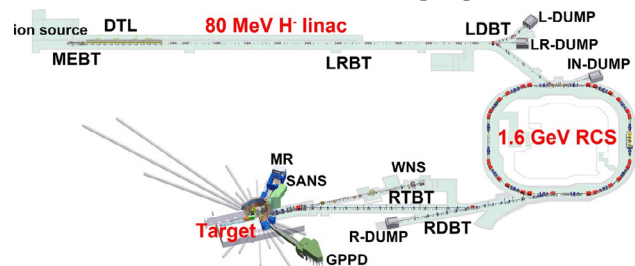


Figure 1: Schematics of the CSNS complex.

In this paper, the performance and some beam loss experiments of our IC BLMs are presented. The relevant Monte Carlo simulations with FLUKA are also executed to verify the experiments, simulates the induced current of different loss scenarios and then evaluates the suitability of electronics, and provide the basis of schemes for some special detections, e.g., the beam-loss detection in the low-energy section of linac for a proton accelerator based on the moderated secondary neutrons.

THE CSNS IC BLM

The schematic and the photograph of the CSNS IC BLM are shown in Fig. 2. The sensitive volume is the tube-like region enclosed by the outer and inner electrode with an effective length of 17.4 cm. The working gas is a mixture of argon and nitrogen with a volume ratio of 70:30 at a total pressure of 1 atm. The standard bias voltage is set to be -2100 V which falls well in the intermediate part of the plateau tested by the ⁶⁰Co source in our previous research [9]. The high voltage is applied on the outer electrode, while electrons are collected on the inner electrode. All electrodes and coverages of BLMs are made of stainless steel, and the insulators are made of alumina ceramics.

*This work is supported by the National Natural Science Foundation of China (Grants No. 11575219, No. 11705215, and No. 11805220).

[†] yangt@ihep.ac.cn

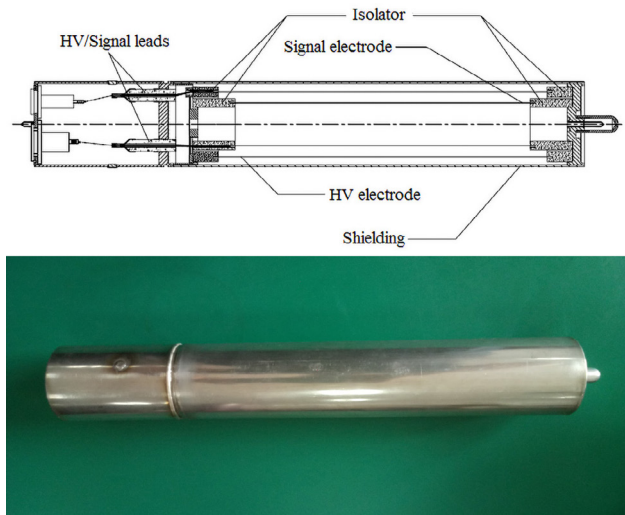


Figure 2: The schematic and the photograph of the CSNS IC BLM.

Beam losses can generally be categorized into the slow loss (regular loss) and fast loss (irregular loss) [3]. The slow losses can be caused by various effects: Touschek effect, collisions, transversal and longitudinal diffusion, residual gas scattering, beam instability, etc. The slow losses are typically not avoidable due to the intrinsic characteristics of beam transport. The fast losses are often caused by the beam misalignment or some operation failures, such as the fault of the rf or magnet power supply system, which may cause serious damage to accelerator components.

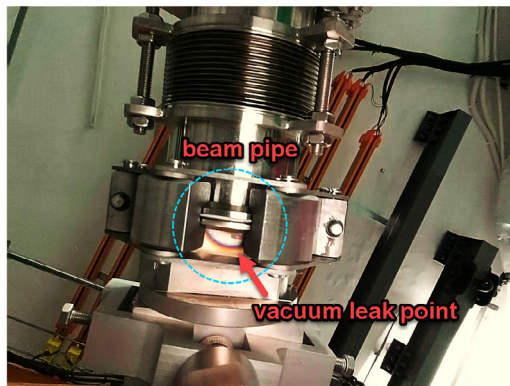
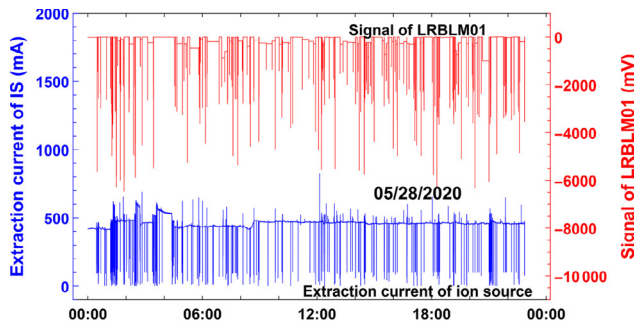


Figure 3: Two typical beam loss categories at the CSNS. The top plot depicts the regular loss caused by the beam instability originated from the sparking of the ion source, and the bottom photo shows an irregular beam loss event leading to a vacuum leak accident at the CSNS LRBT part.

According to the operation experiences at the CSNS, the most frequent causes of regular beam loss are beam instability, residual gas scattering, and space charge effects, while the most frequent cause of irregular loss is the failure of the magnet power supply system. Figure 3 shows two typical beam loss categories at the CSNS. The top plot presents a BLM signal versus the synchronous extraction-current signal of the ion source, which apparently reveals the time relevance of the BLM signal on the beam instability originated from the sparking of the ion source. The bottom photo shows an irregular beam loss event leading to a vacuum leak accident caused by the wrong setting of the switch magnet at the CSNS linac to ring beam transport line (LRBT), which caused a partial melting in the beam pipe and led to a vacuum leak accident.

THE BEAM LOSS EXPERIMENT IN THE MIXED RADIATION FIELD

A good way to validate Monte Carlo simulations and test the sensitivity of BLMs is to create an intentional controlled beam loss and record the monitor responses. Figure 4 depicts the experiment layout of the beam loss detection in the temporary beam diagnostic system during the project construction. The diagnostic system includes a double-slit type emittance monitor and a Faraday cup. The H^- beam energy was ~ 21.67 MeV, and the current was ~ 10 mA. Moving the emittance monitor could generate variable beam losses, and the lost beam current was obtained by the subtraction value of the currents measured by the forward and backward beam current transformers (CTs).

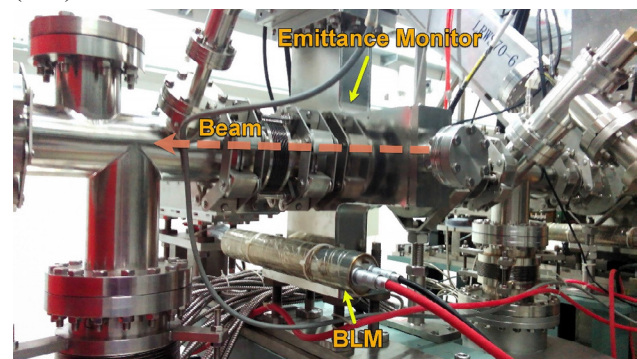


Figure 4: The experiment layout of the controlled beam loss detection using an emittance monitor in the temporary beam diagnostic system during the projection construction.

During the experiment, the emittance monitor was moved in the x -direction to intercept the beam. The simulation results of energy deposition in BLM are finally normalized to the ionization current according to the lost beam current. H^- ions cannot be defined in FLUKA, here we treat the H^- ion as proton in simulations because the two electrons energy of H^- ion (~ 11.9 keV) is rather small compared to the proton energy. The two electrons mainly undergo the ionization energy loss process nearby the loss location, and thus the contribution of stripped electrons to the BLM signal could be neglected.

Content from this work may be used under the terms of the CC BY 3.0 licence (© 2021). Any distribution of this work must maintain attribution to the author(s), title of the work, publisher, and DOI

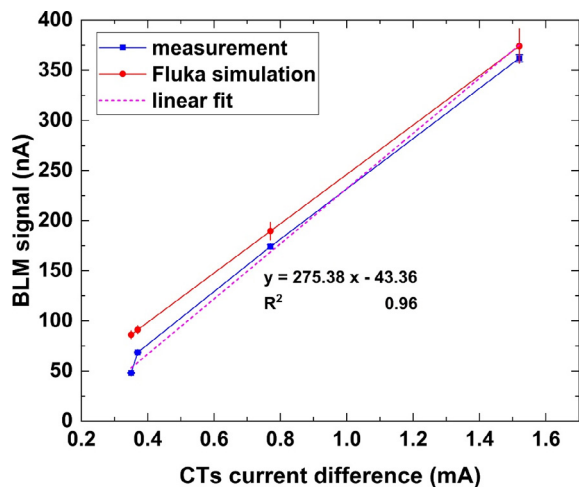


Figure 5: Experimental and simulated BLM signal in the mixed radiation field generated by the movable emittance monitor.

Figure 5 shows the experimental and simulated BLM signal, as can be seen, simulations are basically consistent with the experimental results, and both of which present an approximate linear relation with the lost beam current. Applying the two-steps method in FLUKA, the signal contribution of each particle can be obtained. The result indicates that the secondary photons induced by the beam loss dominate the signal (~85%) for this experiment configuration.

MONTE CARLO SIMULATIONS FOR THE BEAM LOSS RESPONSES

Different loss scenarios are assumed to evaluate the BLM responses, which mainly involves the beam loss on the drift tube in the linac part, loss on the beam pipe of the straight section, quadrupole, and dipole in the RCS part. The uniformly distributed and localized losses are assumed as the two main loss patterns in simulations. Figure 6 illustrates the loss scenarios. The impact angle takes the value of 1 mrad for the scenario I~V. Scenarios II and III simulate the BLM responses of uniform regular losses due to the residual gas scattering, space charge effect, or beam instability, etc. Scenario I, IV, and V simulate responses of localized losses due to aperture limitations. Scenario VI simulates responses of an irregular loss caused by a malfunction of the bending magnet. The lost-particle direction of scenario VI is parallel to the tangential direction of the beam orbit at the entrance of the dipole, which corresponds to an irregular beam loss caused by the beam misalignment or magnet malfunction. Beam energy ranges from 3~80 MeV in the linac part, and from 80~1600 MeV in the RCS part. The quadrupole and dipole magnet for simulations are the frequently used types (RCS206Q, RCS160B) in the RCS part of CSNS.

In order to obtain the macroscopic ionization current responses of BLMs in different scenarios, the responses per lost primary should be multiplied with the beam loss intensity. 1 W/m for a uniformly distributed beam loss is usually considered for most proton accelerators as a

threshold. Consequently, the beam loss rate is assumed to be 1 W/m for scenario II and III corresponding to a uniform loss in the RCS part. While a 0.1% loss is assumed for scenarios I, IV, and V corresponding to a localized loss. The full loss of beam bunch for scenario VI is a hypothetical extreme case, which represents the worst possible accident caused by the failure of the bending-magnet power supply system.

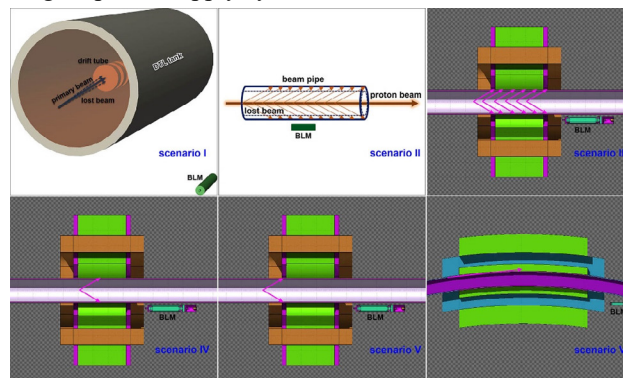


Figure 6: Calculation models of the assumed beam loss scenarios.

The simulated current results for different beam loss scenarios are shown in Fig. 7, and the dashed lines correspond to the corrected current due to the space charge effects. The current for 0.1% loss of scenario I increases with the beam energy and ranges from 0.25 to 2222.09 pA. Although simulations get a positive result for beam energy below 20 MeV, however, due to the sensitivity of electronics (200 pA~20 μA), this beam loss signal couldn't be efficiently detected if the loss rate is very low. In practice, beam loss can be hardly detected for beam energy below 20 MeV during the actual machine operation in CSNS, which is consistent with the simulated results.

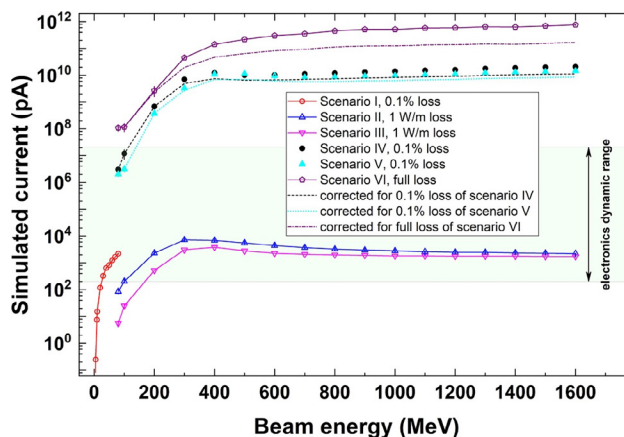


Figure 7: Simulated ionization current for scenarios with the corresponding loss rate. The dashed lines correspond to the corrected current due to the space charge effects.

Considering 200 pA~20 μA the dynamic range of the BLM electronics used in CSNS, BLMs could detect a 0.1% loss level in the CSNS DTL part for beam energy higher than 20 MeV. The simulated current for 1 W/m loss of sce-

nario II~III increases first and then declines with the increase of beam energy, and the current range falls within the electronics dynamic range and in the order of nA except for the beam energy below ~200 MeV. The loss rate of 1W/m means fewer protons for higher beam energy, which corresponds to the slight decline tendency for the 1 W/m loss of scenario II~III. In addition, the ionization rates of scenario I~III with the respective loss rates are far below the critical value $\sim 9.82 \times 10^7$ ions/(cm³·μs) [9], so the current correction due to the space charge effect is needless.

Current responses increase first and then reach a plateau for 0.1% loss of scenario IV~V and full loss of scenario VI. The simulated current for scenario IV and V with 0.1% loss is far beyond the upper limit of input of electronics except for the beam energy below 200 MeV, which however is not a serious issue from a monitoring perspective since this over-threshold signal will trigger the machine protection system to shut down the beam. Disregarding the saturation of electronics, the ionization rate already exceeds the critical value for the three scenarios with the corresponding loss rates when the beam energy is greater than 200~300 MeV, meanwhile, space charge effects begin to play an important role. The dashed lines depict the corrected currents, the collection efficiency declines from 0.70 to 0.53 for scenario IV with 0.1% loss when the beam energy rises from 300 MeV to 1.6 GeV, and it declines from 0.85 to 0.59 for scenario V with 0.1% loss within the same energy range. While for the case of full loss of scenario VI, the collection efficiency declines from 0.89 at 200 MeV to 0.22 at 1.6 GeV. The loss rate on the order of $\sim 10^{-5}$ in one bunch for scenario IV~VI will give a current within the electronics dynamic range, nevertheless, this loss rate would not bring about the space charge effects.

BEAM LOSS DETECTION IN THE LOW-ENERGY SECTION OF THE LINAC

Beam loss detection in the low energy section of CSNS linac (i.e., <20 MeV) is a difficult task using the Ar/N₂ IC since the thick DTL tank (~4.2 cm) has a significant shielding effect on the secondary particles. However, neutrons will leak out of the tank, which may be easier to be detected if suitable neutron converters are selected.

We design an easily assembled and validated scheme to do this research, which mainly employs an IC filled with BF₃ gas and a neutron moderator. Figure 8 depicts the experimental layout and the FLUKA geometric model of the two types of BLMs installed near the DTL tank. BLMs are installed at 2/3 of the first tank length where the nominal beam energy is about 15 MeV. The BF₃ (96%-enriched ¹⁰B) monitor is enclosed by a 7.5-cm-thick HDPE moderator. The monitors' responses are acquired to validate the feasibility of the scheme.

The energy deposition in the sensitive volume of two BLMs given by FLUKA is respectively 0.1335 (±2.1%) eV/primary and 1.115×10^{-4} (±7.1%) eV/primary for the BF₃ and Ar/N₂ BLM. Thus the beam loss signal of the BF₃ monitor is about 1197 (±89) times that of Ar/N₂ BLM, which is a considerable increasement for the signal.

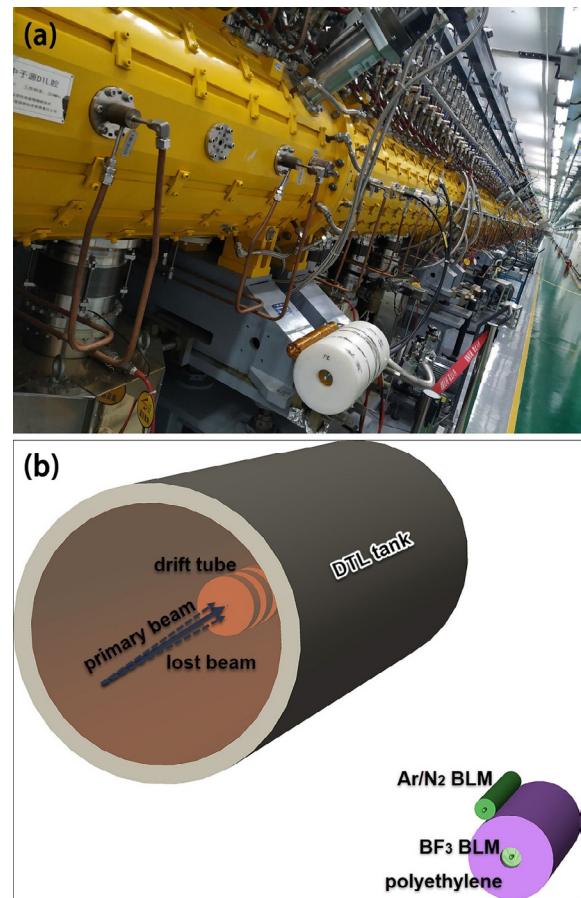


Figure 8: (a) Experimental layout of two types of BLM installed at the first tank of DTL, and (b) the geometric model implemented in FLUKA.

In order to validate the signal ratio of beam loss for the two types of BLM experimentally, we intentionally mismatch the magnet parameters to generate a beam-orbit distortion in a single-shot mode. The waveforms in a loss event are shown in Fig. 9. The Ar/N₂ monitor presents an observable beam loss signal, while the waveform of the BF₃ monitor reaches an oversaturated level. The saturation region of the BF₃ signal could be complemented using the CR-(RC)ⁿ model [10]. The fitting amplitude is respectively 149.5 (±2.0) V for the BF₃ monitor and 91 (±0.87) mV for the Ar/N₂ monitor. The signal of the BF₃ monitor is about 1642 (±27) times higher than that of the Ar/N₂ monitor, which is approximately consistent with the FLUKA simulation in the order of magnitude. The difference is caused by the uncertainty of the actual beam loss. Through simulations and experiments, it demonstrates that the detection of thermal neutrons is an effective way to detect the beam loss in the low energy section of a proton accelerator.

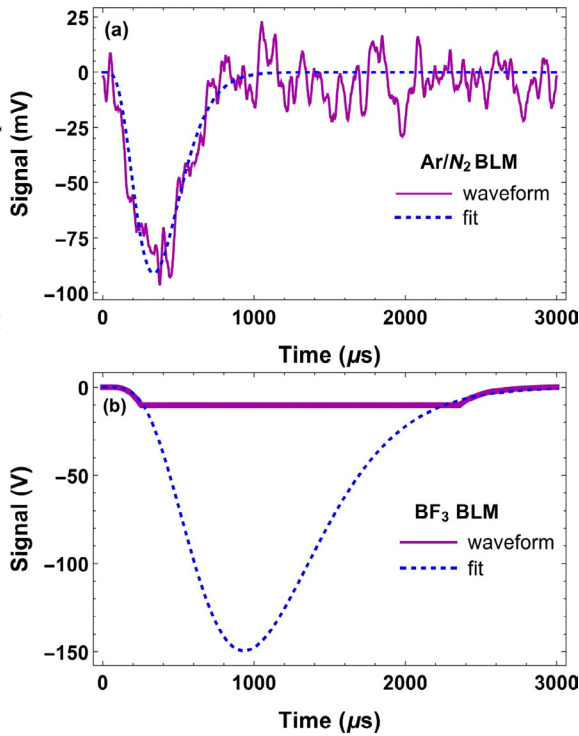


Figure 9: The experimental waveforms of the beam loss signal and the waveform fit in a controlled beam loss event for the (a) Ar/N₂ BLM and (b) BF₃ BLM.

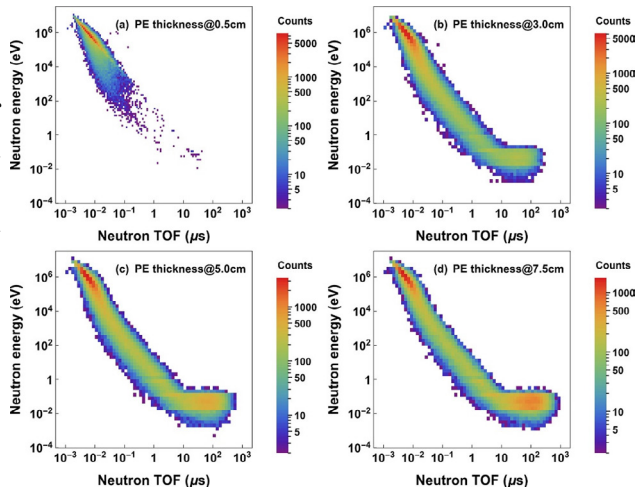


Figure 10: The number of neutrons arriving in the BF₃ monitor plotted versus the neutron TOF and energy in a 2D histogram. The amount of lost protons is 10¹¹.

Figure 10 illustrates a 2D histogram of neutron arriving in the BF₃ monitor as a function of the neutron time of flight (TOF) and the neutron energy. A thermal neutron zone emerges as increasing the PE thickness as seen from Fig. 10, and the neutron TOF roughly ranges from ~ns to hundreds of μs depending on the HDPE thickness. Similar experimental results of the time responses have been reported for the slow-module of neutron sensitive BLM system in ESS, which also presents a maximum time-delay of a few hundreds of μs caused by the moderator layer [11]. The moderator has a delay effect on the beam loss signal, which is caused by the thermalization and migration

process of neutrons [12], and a long delay time is unfavorable for the machine protection, so the moderator thickness should be optimized to balance the detection efficiency and the signal delay in the future applications.

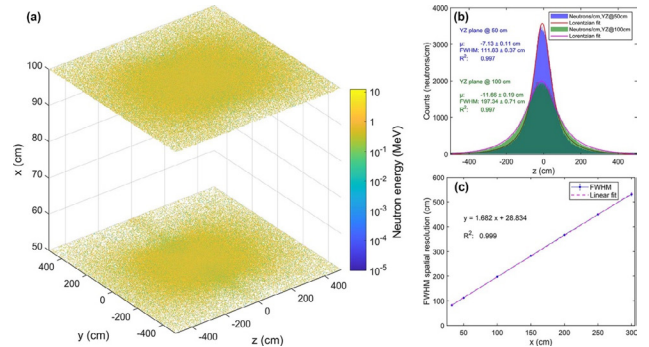


Figure 11: (a) The neutron hit maps on the YZ plane respectively at 50 and 100 cm for the number of lost particles set as 10⁹, (b) the neutron one-dimensional distribution by projecting the 2D hit maps on the z-axis, and (c) the spatial resolution of neutron distribution vs the positions of YZ plane.

Multiple scattering of neutrons will lead to a nonnegligible uncertainty for the loss location by the detection of neutrons. Therefore, the spatial resolution of the source-position of beam loss should be investigated. The problem is simplified in simulation by placing several planes at different positions out of the linac DTL to score the neutron hit positions. The planes are perpendicular to the x-axis with a size of 10×10 m². The beam energy is set to be 15 MeV and the loss position is set at z=0 with a loss angle of 1 mrad. Figure 11 shows the hit maps of secondary neutrons induced by 10⁹ lost primaries and the neutron distribution along the z-axis direction. Neutrons spread wider on the YZ plane at 100 cm compared to 50 cm, which implies that a better spatial resolution can be obtained for a neutron-sensitive BLM closer to the DTL tank. The full width at half maximum (FWHM) is adopted as the spatial resolution. The spatial resolution is respectively 111.83 cm and 197.34 cm for the YZ plane at 50 cm and 100 cm. Figure 11(c) reveals a linear relation of the spatial resolution with locations of the YZ plane. In our experimental configurations, the simulated spatial relation is ~2 m.

CONCLUSION

Beam loss detection is one of the most important issues in a proton accelerator. This paper presents the experimental and Monte Carlo studies for BLMs used in CSNS. We have executed the beam loss measurement in a mixed radiation field with a moveable slit-type emittance monitor on the temporary test stand during the CSNS project construction. The BLM responses in several assumed beam loss scenarios from the linac DTL to the RCS part in the CSNS are also performed, which gives a rough dynamic range of BLM and the signal tendency with the increase of beam energy. The ionization-current responses are obtained according to different loss scenarios

Content from this work may be used under the terms of the CC BY 3.0 licence (© 2021). Any distribution of this work must maintain attribution to the author(s), title of the work, publisher, and DOI

and rates, and the space charge effects are also taken into account. In addition, we study the beam loss monitoring through detection of the moderated neutrons in the low energy section of the DTL part where the low fluences of secondary particles bring out the detection difficulty. The BF₃ monitor was adopted to detect neutrons in the secondary radiation field. Both simulation and experiment show the signal of the BF₃ monitor is about three orders of magnitude higher than that of Ar/N₂ monitor. Finally, the spatial resolution for the neutron-based beam loss detection is estimated from the distribution of secondary neutrons.

REFERENCES

- [1] J. Wei *et al.*, “China Spallation Neutron Source: Design, R&D, and outlook”, *Nucl. Instrum. Methods Phys. Res., Sect. A*, vol. 600, pp. 10-13, 2009.
- [2] A. Lechner *et al.*, “Energy Deposition Studies for Fast Losses during LHC Injection Failures”, in *Proc. 4th Int. Particle Accelerator Conf. (IPAC'13)*, Shanghai, China, May 2013, paper TUPFI027, pp. 1397-1399.
- [3] K. Wittenburg, “Beam loss monitors”, CERN, Geneva, Switzerland, Rep. CERN-2009-005, 2009.
- [4] A. Smolyakov, E. Mustafin, N. Pyka, and P. J. Spiller, “Radiation Damage Studies for the Slow Extraction from SIS100”, in *Proc. 11th European Particle Accelerator Conf. (EPAC'08)*, Genoa, Italy, Jun. 2008, paper THPP102, pp. 3602-3604.
- [5] E. B. Holzer *et al.*, “Beam Loss Monitoring System for the LHC”, in *Proc. IEEE Nuclear Science Symposium*, Fajardo, PR, Oct. 2005, p. 1052.
- [6] D. Gassner, P. Cameron, C. Mi, and R. L. Witkover, “Spallation Neutron Source Beam Loss Monitor System”, in *Proc. 20th Particle Accelerator Conf. (PAC'03)*, Portland, OR, USA, May 2003, paper WPPB017, p. 2447.
- [7] L. Tchelidze, H. Hassanzadegan, A. Jansson, and M. Jarosz, “Beam Loss Monitoring at the European Spallation Source”, in *Proc. 2nd Int. Beam Instrumentation Conf. (IBIC'13)*, Oxford, UK, Sep. 2013, paper WEPC45, pp. 795-798.
- [8] R. Witkover, E. Zitvogel, and R. Michnoff, “RHIC Beam Loss Monitor System Design”, in *Proc. 17th Particle Accelerator Conf. (PAC'97)*, Vancouver, Canada, May 1997, paper 8P067, p. 2218.
- [9] T. Yang *et al.*, “Experimental studies and Monte Carlo simulations for beam loss monitors”, *Phys. Rev. Accel. Beams* vol. 24, p. 032804, 2021.
- [10] G. F. Knoll, *Radiation Detection and Measurement*. New York, NY, USA: John Wiley & Sons, Inc., 2010.
- [11] L. Segui *et al.*, “A Micromegas Based Neutron Detector for the ESS Beam Loss Monitoring”, in *Proc. 7th Int. Beam Instrumentation Conf. (IBIC'18)*, Shanghai, China, Sep. 2018, pp. 211-214. doi:10.18429/JACoW-IBIC2018-TUPA02
- [12] D. G. Cacuci, *Handbook of Nuclear Engineering*. Boston, MA, USA: Springer, 2010.